Monatsh Chem (2010) 141:671–675
DOI 10.1007/s00706-009-0240-5

ORIGINAL PAPER

Formation of the silylene-bridged complex $Fe_2(CO)_6(\mu_2\text{-}SiCl_2)_3$ from *cis*-$Fe(CO)_4(SiCl_3)_2$: an experimental and computational study

Van An Du · Gregor N. Stipicic · Maria Bendova · Ulrich Schubert

Received: 5 November 2009 / Accepted: 15 December 2009 / Published online: 16 January 2010

Abstract Thermolysis of *cis*-$Fe(CO)_4(SiCl_3)_2$ results in the formation of the novel compound $Fe_2(CO)_6(\mu_2\text{-}SiCl_2)_3$, which was characterized by single crystal X-ray diffraction. Density functional theory calculations were carried out to elucidate possible reaction steps leading to the formation of $Fe_2(CO)_6(SiCl_2)_3$, including CO dissociation and chlorine abstraction by a $SiCl_3$ radical generated from homolytic Fe–Si bond cleavage involving a singlet–triplet intersystem crossing.

Keywords Metal silyl complexes · Homolytic bond cleavage · Bridging silylene ligand · DFT calculations

Introduction

Applications of transition metal silicides include direct band-gap semiconductors as catalysts or in photonics [1]. An interesting option for the synthesis of metal silicide films or nanoparticles is thermolysis of metal silyl complexes as molecular single-source precursors. For example, iron silicide films were prepared by MOCVD processes from *cis*-$Fe(CO)_4(SiCl_3)_2$ (**1**). Based on photoelectron spectra and theoretical calculations, Zybill et al. proposed intramolecular $SiCl_4$ elimination and concomitant formation of an iron silylene complex as initial mechanistic steps during the generation of iron silicide [2, 3]. We recently reported that in solution and in the presence of hexamethylphosphoric triamide (HMPA), the ionic complex $[SiCl_3(HMPA)_3]^+[Fe(CO)_4SiCl_3]^-$ is formed from **1** by heterolytic cleavage of an iron–silicon bond [4]. In the present contribution, we re-examine the gas-phase decomposition of **1** and re-calculate the initial elementary reaction steps by DFT methods.

V. A. Du · M. Bendova · U. Schubert (✉)
Institute of Materials Chemistry,
Vienna University of Technology,
Vienna, Austria
e-mail: uschuber@mail.zserv.tuwien.ac.at

G. N. Stipicic
Institute of Applied Synthetic Chemistry,
Vienna University of Technology,
Vienna, Austria

Results and discussion

The experiments by Zybill et al. [3] were carried out under CVD conditions, i.e., the decomposition of **1** and formation of iron silicides occurred at silicon or glass surfaces. A clear dependence on the substrate surface was observed, as β-$FeSi_2$ films were formed on a Si(100) surface and polycrystalline cubic FeSi on a Pyrex glass substrate. In an attempt to prepare iron silicide nanoparticles, we carried out thermolysis of **1** under different conditions. To this end, solid **1** was sealed in a glass vial under argon and heated to 350 °C for 30 min. After cooling to room temperature, the vial was opened, and $FeCl_2$ and yellow, needle-shaped crystals of $Fe_2(CO)_6(SiCl_2)_3$ (**2**) were obtained as the only solid compounds. A silicide phase or residual starting compound was not observed. Although we did not analyze the gaseous products, theoretical calculations (see below) and photoelectron spectroscopy studies by Zybill et al. [2, 3] suggest that CO and $SiCl_4$ are also formed. Thus, the overall reaction could be

$$5Fe(CO)_4(SiCl_3)_2 \rightarrow FeCl_2 + 2Fe_2(CO)_6(SiCl_2)_3 + 4SiCl_4 + 8CO$$

Complex **2** crystallized in the highly symmetric space group $P6_3/m$ (Fig. 1). The iron atoms are octahedrally

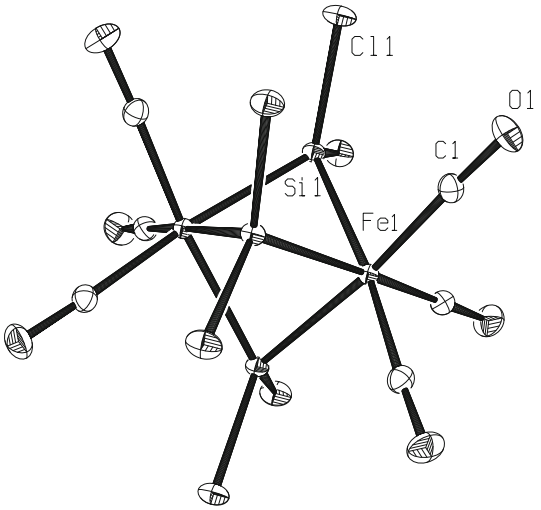

Fig. 1 ORTEP plot of $Fe_2(CO)_6(SiCl_2)_3$ (**2**). Selected bond distances (pm) and angles (deg): Fe(1)–Fe(1)* 272.6(8), Fe(1)–C(1) 181(1), Fe(1)–Si(1) 229.7(4), Si(1)–Cl(1) 204.2(6), Si(1)–Fe(1)–Si(1)* 72.805(4), Fe(1)–Si(1)–Cl(1) 120.58(1) (Atoms marked with an *asterisk* are symmetry-related)

coordinated with a facial arrangement of the carbonyl ligands and three bridging dichlorosilylene ligands connecting the two metal centers. In comparison to the known crystal structure of $Fe_2(CO)_6(\mu_2\text{-SiClMe})(\mu_2\text{-SiMe}_2)_2$ (Fe–Fe 270.5 (1) pm, average Fe–Si = 232.2(2) pm) [5], which has been obtained in low yield by photochemical reaction of $Fe_2(CO)_8(SiMe_2)_2$ with $Fe(CO)_4(H)SiMe_2C1$ [6], the Fe–Fe distance (272.6(8) pm) in **2** is only slightly longer, and the Fe–Si distance (229.7(4) pm) slightly shorter. The structure of **2** is related to the prototypical $Fe_2(CO)_9$ with the same point group (D_{3h}). Replacement of the three silylene ligands by three bridging carbonyl ligands results in a significantly shorter Fe-Fe distance of 252.3(8) pm [7].

The IR spectrum of **2** shows two strong absorptions in the carbonyl region at 2,022 and 2,001 cm^{-1}. Scaled frequencies by a factor of 0.9945 [8] obtained from calculations carried out as part of the computational study reproduce the experimental results with high accuracy (calculated values: 2,029 and 2,001 cm^{-1}).

The different outcome of the thermolysis reaction, compared to that reported by Zybill et al., prompted us to re-calculate possible intermediates for this reaction. We first investigated CO dissociation as a possible initial step in the total reaction. The first bond dissociation energies for *cis*-$Fe(CO)_4(SiCl_3)_2$ (Table 1) are 125.2 kJ/mol for the CO ligand *trans* to CO and 108.4 kJ/mol for the CO ligand *trans* to $SiCl_3$. We were also able to locate transition states for CO ligand dissociation in both cases, $\mathbf{TS_{AB}}$ and $\mathbf{TS_{AC}}$, leading to $Fe(CO)_3(SiCl_3)_2$: the energetic barriers amount to 127.7 and 98.8 kJ/mol (Fig. 2, compound **A** in the calculations corresponds to complex **1**, **B** and **C** denote the

Table 1 First bond dissociation energies and associated barrier heights for $Fe(CO)_4(SiCl_3)_2$

Bond	D_e (kJ mol^{-1})	ΔG_{TS} (kJ mol^{-1})
$Fe–CO_{trans\ CO}$	125.2	127.7 (heterolytic dissociation)
$Fe–CO_{trans\ SiCl3}$	108.4	98.8 (heterolytic dissociation)
$Fe–SiCl_3$	161.2	151.1 (homolytic dissociation)

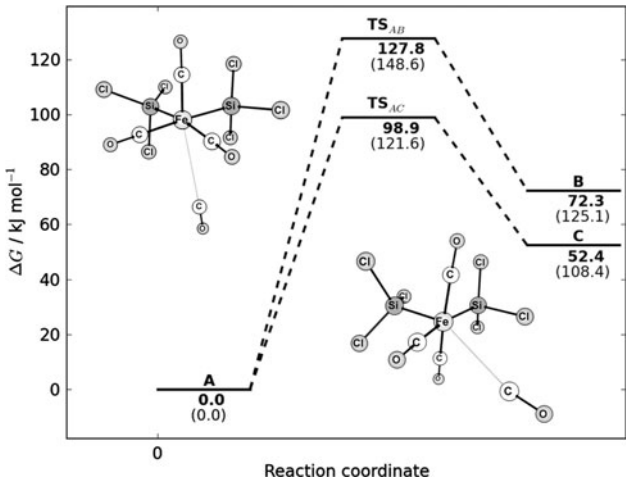

Fig. 2 Gibbs free-energy profile for CO ligand dissociation from **A**. The *numbers in parentheses* are differences in uncorrected electronic energies

products of CO dissociation *cis* or *trans* to $SiCl_3$). This implies both thermodynamic and kinetic labilization of the CO ligands *trans* to the $SiCl_3$ ligands, which is in excellent agreement with the experimental observation that PPh_3 exclusively substitutes the CO ligands *trans* to the SiR_3 in complexes *cis*-$Fe(CO)_4(SiR_3)_2$ [9, 10].

As previously reported, the Fe–Si bond in **1** is heterolytically cleaved in solution in the presence of HMPA to stabilize the cleaved $SiCl_3^+$ [4]. Such a charge separation is expected to be highly unfavorable in the gas phase, i.e., in the absence of any stabilizing agent. As a matter of fact, a stepwise lengthening of one of the Fe–Si bonds from the calculated equilibrium distance of 245 pm in **A** (with multiplicity 2S + 1 = 1) leads to a continuous increase in energy and an asymptotic approach to the energy of $[(CO)_4FeSiCl_3]^-$ and $SiCl_3^+$ at infinite separation (Fig. 3). Consequently, the energy required for $SiCl_3^+$ dissociation (i.e., on the singlet surface) is very high (Fig. 3).

We were unable to locate a transition state for unimolecular $SiCl_4$ elimination from neutral *cis*-$Fe(CO)_4(SiCl_3)_2$. This is due to an unfavorable interaction between a region of the LUMO with *s*-character at the silicon atom of the $SiCl_3$ group and an orbital of the HOMO with p_z-character on the chloride atom in closest proximity. Nevertheless, Zybill et al. estimated an energy for $SiCl_4$ elimination by a

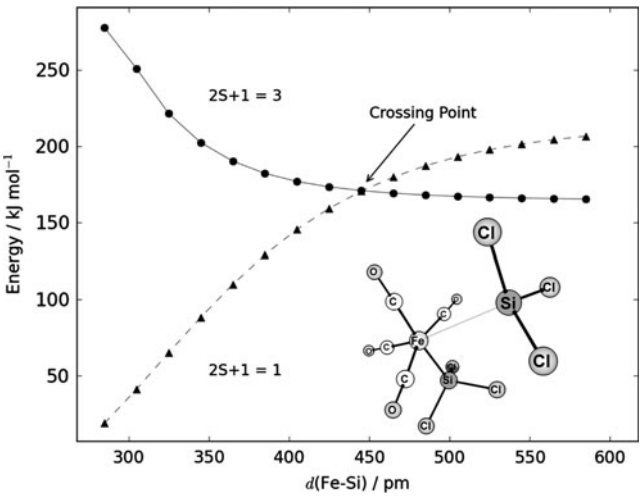

Fig. 3 Pure electronic energy as a function of Fe-Si bond length for both singlet and triplet states (*S* angular spin momentum)

constrained geometry optimization, which is as high as 197 kJ/mol [2, 3]. We re-evaluated this result at the present level of theory and found that a constrained optimization leads to a geometry that unsurprisingly is not a stationary point on the potential energy surface. The vibrational mode corresponding to the observed imaginary frequency is in fact a rotation around one of the Fe-Si bonds.

In light of those findings, a different mechanism is postulated for the elimination of $SiCl_4$ during the thermolysis of **1**. Starting from **A,** we propose a homolytic Fe-Si bond cleavage (Table 1), resulting in a $SiCl_3$ radical as a crucial participant in further mechanistic steps. Chlorine abstraction by $SiCl_3$ radicals has already been the subject of a computational study in a related context [11]. In contrast to heterolytic Fe-Si bond cleavage on the singlet surface, homolytic Fe-Si bond cleavage on the triplet surface (multiplicity $2S + 1 = 3$) is much more favorable, and we were able to approximate the location of the corresponding transition state as a crossing point between the singlet and triplet state by an evaluation of the energy as a function of one of the Fe–Si bond lengths (Fig. 3) [12]. Transition state energies for dissociation reactions are summarized in Table 1. We do not consider Cl_2 or Cl radicals because only $SiCl_4$ and CO were observed in photoelectron spectroscopy studies of the thermolysis reaction of **1** [2, 3].

Two proposed mechanistic pathways leading to the radical species $[(CO)_3FeSiCl_3SiCl_2]$ (**E**) are shown in Fig. 4 (for a graphical representation of the structures, see Fig. 5). Obviously, either CO dissociation or chlorine abstraction by a $SiCl_3$ radical can initially take place. Different transition states are possible for chlorine abstraction, differing only in rotation about the Fe-Si bond. Only the transition states (**TS**) with the lowest barrier are shown in the energy profile in Fig. 5. The calculations led to the conclusion that CO dissociation as a first step ($\mathbf{TS_{AC}}$) is less favorable and associated with a barrier of 98.8 kJ/mol in comparison to transition state $\mathbf{TS_{AD}}$ leading to radical species $(CO)_4FeSiCl_3SiCl_2$ (**D**). The second pathway, i.e., CO abstraction, is characterized by a low energy barrier of 36 kJ/mol (energy of $\mathbf{TS_{DE}}$ relative to **D** in Fig. 5). In summary, the second pathway is more likely, and the overall reaction leading from **A** to **E** is exergonic with –47.7 kJ/mol.

We envision that **E** is a direct precursor for compound **2** after further $SiCl_4$ elimination by recombination with itself, now involving a triplet-singlet intersystem crossing (Fig. 6).

In conclusion, the new dimeric iron complex **2** with three bridging silylene ligands was isolated and unequivocally characterized by single crystal X-ray diffraction. An alternative mechanistic rationale for $SiCl_4$ formation during thermolysis of **1** is proposed based on DFT calculations. The proposed mechanism involves chlorine abstraction by a $SiCl_3$ radical generated from homolytic Fe-Si bond cleavage, involving a singlet-triplet intersystem crossing. We have not investigated whether further thermolysis of **2** results in the formation of iron silicides.

Experimental

All manipulations were carried out under an atmosphere of dry argon using Schlenk-line techniques or using a glove

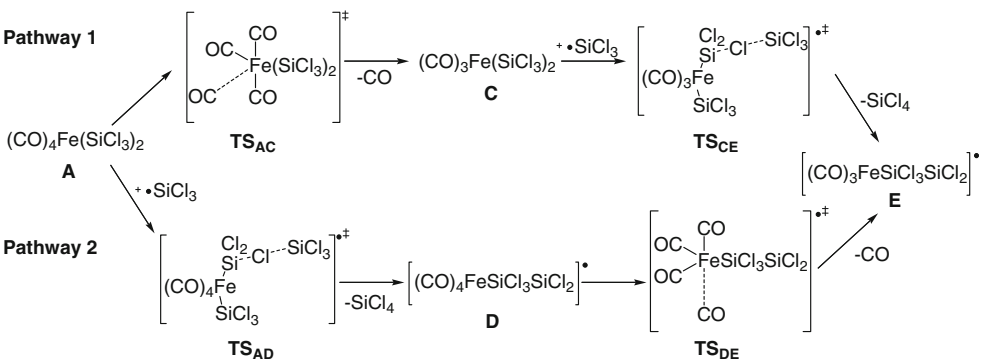

Fig. 4 Possible pathways for the formation of **E**

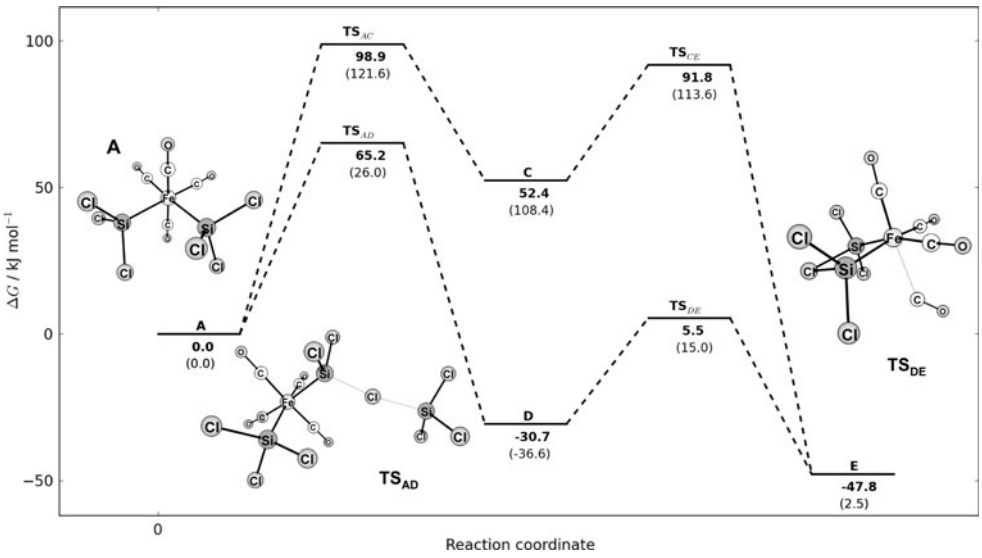

Fig. 5 Reaction profile for two different pathways towards **E**. Gibbs free energies are shown; the *numbers in parentheses* are differences in uncorrected electronic energies

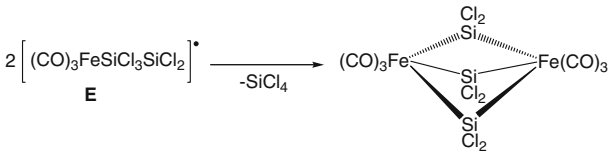

Fig. 6 Proposed recombination of **E** to $Fe_2(CO)_6(SiCl_2)_3$

box. Infrared spectroscopy measurements were performed on a Bruker Tensor 27 spectrometer (32 scans at a resolution of 4 cm^{-1}) using a liquid cell with toluene as a solvent. *cis*-$Fe(CO)_4(SiCl_3)_2$ was prepared by a modified procedure from the literature [13].

Computations were carried out at the BLYP/6-311G (3df)//BLYP/m6-31G(d) level of theory with the pure BLYP density functional [14, 15], employing the triple zeta basis set 6-311 + G(2df) for single point calculations and the double zeta basis set m6-31G(d) [16] in unconstrained geometry optimizations, transition state searches, and frequency calculations on all localized stationary points on the potential energy surface. Electronic energies obtained from single point calculations were corrected with unscaled harmonic zero point energies and thermal corrections at $T = 298.15$ K obtained at the lower level of theory, and are therefore reported as Gibbs free energies. All calculations were carried out with the Gaussian 03 program package [17], and basis sets were retrieved from the EMSL Basis Set Exchange Library [18].

Synthesis of $Fe_2(CO)_6(SiCl_2)_3$

A 20-cm^3 glass vial was charged with 0.20 g of *cis*-$Fe(CO)_4(SiCl_3)_2$ (0.46 mmol) and sealed under argon atmosphere. The vial was heated in a furnace to 350 °C for 30 min with a heating rate of 2 °C/min. After cooling to room temperature, $FeCl_2$ and yellow, needle-like crystals of **2** were obtained. Yield: 0.03 g (12%); IR (toluene): $\bar{\nu} = 2,022(\text{vs}), 2,001(\text{s})$ (CO) cm^{-1}.

X-ray structure determination

Single crystal X-ray diffraction experiments were performed on a Bruker-AXS APEX diffractometer with a CCD area detector and a crystal-to-detector distance of 5.5 cm using graphite-monochromated MoK_α (Table 2) radiation ($\lambda = 71.073$ pm) at 100 K. The data collection covered a full sphere of the reciprocal space by recording eight sets of exposures. Each exposure took 10 s and covered 0.3° in ω. The data were corrected for polarization

Table 2 Crystallographic and structural parameters of $Fe_2(CO)_6(SiCl_2)_3$

Empirical formula	$C_6Cl_6Fe_2O_6Si_3$
M_r	576.73
Crystal system	Hexagonal
Space group	$P6_3/m$
a (pm)	941.4 (1)
c (pm)	1,175.2(3)
V (10^6 pm^3)	902.0(3)
Z	2
μ_{calc} (g cm^{-3})	2.123
μ (mm^{-1})	2.714
Crystal size (mm^3)	0.76 × 0.08 × 0.07
θ range (deg)	2.50–30.50
Reflections coll./unique	10,307/969
Data/parameters	969/40
GOF on F^2	1.135
R [$I > 2\sigma(I)$]	0.013
wR_2 [$I > 2\sigma(I)$]	0.035
Largest diff. peak/hole (e $Å^{-3}$)	0.278/−0.210

and Lorentz effects, and an empirical absorption correction (SADABS) was applied. The cell dimensions were refined with all unique reflections. The structure was solved with direct methods (SHELXS–97) [19]. Refinement to convergence was carried out with the full-matrix least-squares method based on F^2 (SHELXS–97) with anisotropic structure parameters for all atoms.

CCDC 753054 contains the supplementary crystallographic data for this paper. These data can be obtained free of charge from The Cambridge Crystallographic Data Center via http://www.ccdc.cam.ac.uk/data_request/cif.

Acknowledgments This work was supported by Shell Corp., The Netherlands.

References

1. Derrien J, Chevrier J, Lethanh V, Mahan JE (1992) Appl Surf Sci 382:56
2. Huang H, Zybill CE, Luo L, Hieringer W, Huang HH (1998) Organometallics 7:5825
3. Zybill CE, Huang W (1999) Inorg Chim Acta 291:380
4. Du VA, Baumann SO, Stipicic GN, Schubert U (2009) Z Naturforsch B 64:1553
5. Simons RS, Tessier CA (1995) Acta Cryst C 51:1997
6. Schmid G, Welz E (1979) Z Naturforsch B 34:929
7. Cotton FA, Troup JM (1974) J Chem Soc Dalton Trans 800
8. Scott AP, Radom L (1996) J Phys Chem 100:16502
9. Pomeroy RK, Wijesekera KS (1980) Inorg Chem 19:3729
10. Schubert U, Knorr M, Strasser C (1991) J Organomet Chem 411:75
11. Bottoni A (1998) J Phys Chem A 102:10142
12. Harvey NJ (2001) Spin-forbidden reactions in transition metal chemistry. In: Cundari TR (ed) Computational organometallic chemistry. Marcel Dekker, New York, p 291
13. Novak I, Huang W, Luo L, Huang HH, Ang HG, Zybill CE (1997) Organometallics 16:1567
14. Becke AD (1988) Phys Rev A 38:3098
15. Lee C, Yang W, Parr RG (1988) Phys Rev B 37:785
16. Alexander MV, Baker J, Pulay P (2003) J Chem Phys 118:7775
17. Frisch MJ, Trucks GW, Schlegel HB, Scuseria GE, Robb MA, Cheeseman JR, Montgomery Jr JA, Vreven T, Kudin KN, Burant JC, Millam JM, Iyengar SS, Tomasi J, Barone V, Mennucci B, Cossi M, Scalmani G, Rega N, Petersson GA, Nakatsuji H, Hada M, Ehara M, Toyota K, Fukuda R, Hasegawa J, Ishida M, Nakajima T, Honda Y, Kitao O, Nakai H, Klene M, Li X, Knox JE, Hratchian HP, Cross JB, Bakken V, Adamo C, Jaramillo J, Gomperts R, Stratmann RE, Yazyev O, Austin AJ, Cammi R, Pomelli C, Ochterski JW, Ayala PY, Morokuma K, Voth GA, Salvador P, Dannenberg JJ, Zakrzewski VG, Dapprich S, Daniels AD, Strain MC, Farkas O, Malick DK, Rabuck AD, Raghavachari K, Foresman JB, Ortiz JV, Cui Q, Baboul AG, Clifford S, Cioslowski J, Stefanov BB, Liu G, Liashenko A, Piskorz P, Komaromi I, Martin RL, Fox DJ, Keith T, Al-Laham MA, Peng CY, Nanayakkara A, Challacombe M, Gill PMW, Johnson B, Chen W, Wong MW, Gonzalez C, Pople JA (2004) Gaussian 03, Revision C.02, Gaussian Inc Wallington CT
18. Schuchardt KL, Didier BT, Elsethagen T, Sun L, Gurumoorthi V, Chase J, Li J, Windus TL (2007) J Chem Inf Model 47:1045
19. Sheldrick GM, SHELXS/L -97 (1997) Programs for crystal structure determination. University of Göttingen, Göttingen, Germany